Separation of light confinement and absorption sites for enhancing solar water splitting

Received 02nd September 2015,
Accepted 250th November 2015

DOI: 10.1039/C5TA06972F
www.rsc.org/

A. Niv,[a†] M. Gross Koren,[b] H. Dotan,[b] G. Bartal,[c] and A. Rothschild[b†]

Lambertian light trapping is a well-known method for enhancing the light harvesting efficiency of solar cells. Since it is based on ray optics, it is conventionally considered as inapplicable for subwavelength ultrathin films. Here we show a way around this limitation by separating the light confinement and absorption sites within the stack of materials comprising the entire cell. We demonstrate this approach for ultrathin film hematite (α-Fe_2O_3) photoanodes designed for renewable hydrogen production via solar water splitting. Attaching a Lambertian back reflector (that is, a white scattering sheet) to the backside of the cell results in a photocurrent enhancement of 25% to 30%, depending on the hematite thickness, in comparison to the same cell with a specular back reflector (i.e., a mirror). Theoretical analysis suggests that even higher enhancement may be possible, exceeding 40% in some cases, if light escape through the cell edges could be prevented. The proposed approach is not material-specific and can be readily implemented in other materials and other types of solar cells. Another advantage of this approach is that the light management is achieved using simple commercial products, making the proposed approach cost-effective and easy to implement in a variety of solar cells and photodetectors.

Introduction

The need for cost-effective and sustainable solutions for storing intermittent renewable energy has spurred a growing interest in artificial photosynthesis and solar fuels.[1,2] In this regard, hematite (α-Fe_2O_3) is a promising photoanode candidate for solar hydrogen production via photoelectrochemical (PEC) water splitting, mainly due to its nearly optimal bandgap of 2.1 eV, stability in alkaline aqueous solutions, and vast abundance.[3,4,5] Hematite, however, also has drawbacks, foremost its fast charge recombination and low mobility of electrons and holes.[6,7] Consequently, the feature size, that is, the film thickness (unless using porous films), in practical hematite photoanodes is limited to several tens of nanometers for the effective collection of the photogenerated minority charges (holes in n-type photoanodes). Unfortunately, this is well below the light penetration depth in hematite, which is about 300 to 500 nm for visible light. The large gap between the optical and charge transport length scales in hematite presents a salient dilemma: Thick hematite photoanodes lose most of their photogenerated charge carriers to recombination, whereas ultrathin films are simply not thick enough to absorb a significant amount of the incident light. Thus, in both cases, the solar to hydrogen conversion efficiency is limited, either by charge recombination or light harvesting, respectively.

Recently we demonstrated a resonant light trapping scheme that exploits the wave-nature of light to tailor the light intensity distribution inside ultrathin hematite films on specular back reflectors.[8] In this case, constructive interference between forward- and backward-propagating waves amplifies the intensity close to the surface of quarter-wave films, thereby maximizing the productive absorption in regions where photogenerated charge carriers reach the surface before recombination takes place, and minimizing the wasted absorption far away from the surface wherein non-radiative recombination prevails. A schematic illustration of the photoanode stack that gives rise to resonant light trapping is depicted in Fig. 1(A). This design, in combination with re-trapping of the back-reflected light via multiple reflections between two specular photoanodes facing each other in a V-shaped cell, enables, in theory, the harvesting of as much as 84% of the photons in the sunlight spectrum (AM1.5G) below the absorption edge of hematite (590 nm) within 20-30 nm thick hematite films on silver-coated substrates. The remaining 16% of the photons are lost to wasted absorption in the silver back reflector. However, in practice, it is difficult to obtain high quality silver back reflectors since the hematite film must be deposited directly on the back reflector in an oxygen atmosphere and at high temperatures in order to achieve the required stoichiometry and crystalline structure. These deposition conditions result in tarnishing of the silver back reflector due to thermal etching.[9] In order to mitigate this problem, TiN and SnO_2 passivation underlayers were applied, but the need to maintain the resonance interference effect limited their thickness to no more than several nanometers, thereby limiting their effectiveness in preventing tarnishing of the silver back reflector.

This challenge motivated us to facilitate a substantial separation between the back reflector and the hematite film, for example, by moving the reflecting layer to the backside of the glass substrate, as illustrated in Fig. 1(B). In this case, a transparent conductive oxide (TCO) electrode, such as fluorinated tin oxide (FTO), serves as an electron current collector. Separating the back reflector from the hematite film resolves the tarnishing problem, but it also diminishes the resonance effect between the forward- and backward-propagating waves because they are no longer coherent after passing through the mm-thick

[a.] *Swiss Institute for Dryland Environmental and Energy Research, Blaustein Institutes for Desert Research, Ben-Gurion University of the Negev, Israel.*
[b.] *Department of Materials Science and Engineering, Technion – Israel Institute of Technology, Haifa 32000, Israel.*
[c.] *Department of Electrical Engineering, Technion – Israel Institute of Technology, Haifa 32000, Israel.*
† Corresponding authors:
aviniv@bgu.ac.il; Tel: +972-86563498; Fax: +972-86596736
avner@mt.technion.ac.il; Tel: +972-4-8294576; Fax: +972-4-8295677

substrate. So the question is how to enhance the productive absorption in the hematite film in the photoanode design shown in Fig. 1(B)?

One of the most effective light-management techniques is the Lambertian light trapping method.[11,12] This method exploits the total internal reflection (TIR) of randomized rays to confine light in the interior of the cell, thereby enhancing the absorption. Careful consideration shows that the average optical path length of randomized rays could be $4n^2$ larger than a single pass through the cell, where n is the refractive index. This suggests that for a low loss material, the absorption could be enhanced by as much as $4n^2$, thus defining the Lambertian limit. For more than three decades, Lambertian trapping has served as a simple yet powerful tool for improving the performance of PV cells. It would be advantageous if this tool could somehow be applied to improve the performance of the ultrathin photoanodes considered in this work.

Offhand, this idea appears to be impossible since the Lambertian light trapping method is based on ray optics, whereas subwavelength optical features, such as the ultrathin hematite photoanodes under consideration here, belong to the realm of wave optics. Indeed, this mismatch has motivated the investigation of advanced light-management techniques based on plasmonics,[12-15] nano-photonics,[16,17] and nano-optics in general.[18-21] Despite the remarkable progress in this field, and although some of these designs are predicted to surpass the Lambertian light trapping limit,[22,23] thus far, none of them rivals the Lambertian light trapping method when it comes to practical utility.[24] The success of the Lambertian light trapping method is due to two main reasons: First, it is stochastic in nature and thus inherently broadband, whereas the other methods rely on either interference or resonance effects. Second, it uses far-field optics, whereas the other methods rely on near-field light-matter interactions that burden the already intricate structure of the device. In addition, light management practiced from afar is of particular interest for the PEC cells considered here due to the corrosive environment in which water splitting takes place, either in alkaline or acidic aqueous solutions.

Here we show that the key to bridging the length scale gap between statistical ray optics and subwavelength ultrathin films lies in the separation of light confinement and absorption sites within the cell. Thus, Lambertian light trapping in the lossless compartments of the cell can enhance the absorption in the subwavelength hematite film. Lambertian light trapping, in this case, is achieved by attaching a highly reflective scattering sheet on the backside of the cell, as shown in Fig 1(B). This work investigates a PEC cell fitted with a Lambertian back reflector, and compares the absorptance and photocurrent of this cell with a counterpart cell fitted instead with a specular back reflector (i.e., mirror).

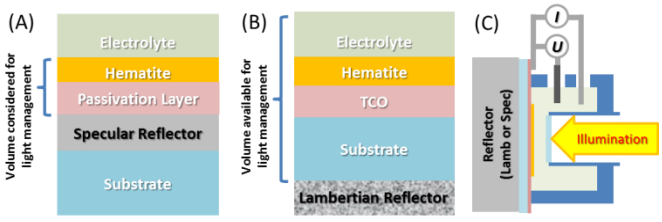

Fig. 1. (A) Schematic illustration of the resonant light trapping design. (B) Schematic illustration of the PEC cell layout that is hereby proposed: The photoactive hematite layer is separated from the back reflector by the transparent substrate. A transparent conductive oxide (TCO) is used as a back-contact in this case. This leaves a large optical lossless volume for implementing the ray-based Lambertian light confinement. (C) Schematic illustration of the PEC cell: Light enters from the right, and I and U denote the current and electrode potential circuitry, respectively. Color coding is otherwise identical to that in panels (A) and (B).

Experimental Results

In order to test our approach, four hematite photoanodes were prepared with film thicknesses of 15, 19, 23 and 30 nm. The films were deposited by pulsed laser deposition (2" PLD Workstation, Surface, GmbH) from a 1 cation% Ti-doped iron oxide target. The films were deposited on fluorinated tin oxide coated glass substrates (1.8 mm thick TEC15 substrates, Pilkington, USA). The target was prepared by a conventional mixed-oxide solid state reaction route, starting from commercial Fe_2O_3 (99.99%) and TiO_2 (99.995%) powders (Alfa Aesar). The powders were mixed in appropriate amounts to obtain a doping level of 1% Ti in Fe_2O_3, ball-milled for 24 h using YTZ milling balls (Tosoh, Japan), and subsequently pressed in a stainless steel mold and sintered in air at 1200°C

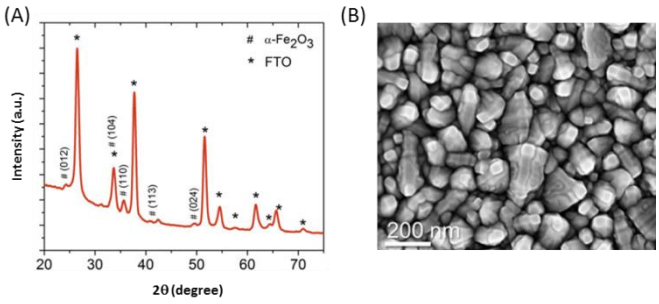

Fig. 2. Typical X-ray diffractogram (A) and high resolution scanning electron micrograph (B) of the thin film hematite photoanodes. Reproduced with permission from Ref. 25 (Cambridge University Press, 2015).

for 12 h, resulting in a target with a relative density of 88%. Thin films were deposited from this target using a PLD workstation equipped with a KrF (λ = 248 nm) excimer laser (COMPexPro 102, Coherent, GmbH). The films were deposited at a laser fluence of 1 J cm^{-2} and a repetition rate of 5 Hz, at a target substrate distance of 70 mm. The depositions were carried out

at a heater set point temperature of 600°C, which corresponds to a substrate temperature of approximately 450°C. Prior to the iron oxide deposition, thin SnO_2 interlayers (estimated thickness of 24-40 nm) were deposited in order to suppress the backward transport of charge carriers from the hematite to the FTO current collector. Subsequently, the iron oxide films were deposited under oxygen flow at a pressure of 25 mTorr. The number of laser pulses was varied to obtain photoanodes with different hematite film thicknesses: 15, 19, 23 and 30 nm. Figure 2 (A) presents a typical XRD diffractogram of the hematite photoanodes. The peaks are labelled with respect to the Bragg reflections from different planes in the Fe_2O_3 hematite phase (α-Fe2O3, JCPDS 01-080-5413) and the SnO_2 rutile phases (JCPDS 01-079-6887). No other peaks are observed, confirming the existence of a single phase hematite film on the FTO-coated glass substrate. Figure 2(B) shows a typical high resolution scanning electron micrograph (Zeiss Ultra Plus) of the same photoanode as in panel (A). The morphology is homogenous across the field of view, indicating uniform coverage of the hematite film over the substrate. Further characterizations of the hematite photoanodes can be found elsewhere.[25]

Since light escape through the cell edges is detrimental for Lambertian light trapping, the photoanodes were made as large as possible (40 mm in diameter) in order to reduce this parasitic loss as much as possible. For the same reason, the thickness of the electrolyte layer in front of the photoanode was minimized to 1 mm by allocation of the front window of the PEC cell. We have found that this gap allowed the undisturbed flow of the chemical reactants and gas products, whereas a narrower gap was found to hinder the electrochemical reaction. A schematic illustration of the PEC cell is given in Fig. 1(C).

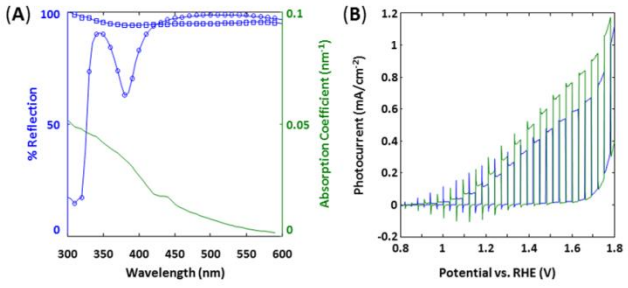

Fig. 3. (A) Normalized reflectance spectra of the specular (blue circles) and Lambertian reflectors (blue squares), and absorption coefficient of the hematite film (green line). (B) Chopped light voltammogram of a 19 nm-thick hematite photoanode; blue and green lines correspond to measurements taken with the specular and Lambertian reflectors attached at the backside of the PEC cell, respectively.

Most importantly, modular construction of the PEC cell enabled easy swapping of the back reflector without changing the cell assembly or its alignment with respect to the light source. Two commercially available reflectors were examined: A diffusive reflector sheet (1 mm thick diffused reflector, a product of Gore) was used as the Lambertian scatterer, while a standard Ag mirror (Thorlabs) was used as a specular mirror (for comparison). The normalized reflectance spectra of the two reflectors are shown in Fig. 3(A). The Ag mirror (circles) displays slightly higher reflectance by as much as 3% over the Lambertian reflector (squares) from the hematite absorption edge at 590 nm and down to 450 nm. At 424 nm, the reflectance of the two reflectors becomes identical, whereas at shorter wavelengths, the reflectance of the Ag mirror drops sharply. In contrast, the Lambertian reflector maintains high reflectance at short wavelengths. The difference in reflectance at shorter wavelengths is not an appreciable problem since the solar simulator does not produce significant power below 400 nm. For later use, we also show in Fig. 3(A) the absorption coefficient of hematite, measured by spectroscopic ellipsometry (VASE Ellipsometer, J. A. Woolam Co.), represented by the green curve. The absorptance of the TEC15 substrate was found to be negligible with respect to that of the hematite film, and therefore, it is not considered here.

Photocurrent measurements were carried out for illumination from a class AAA AM1.5G solar simulator (ABET Technologies). Linear sweep voltammograms were measured in three electrode mode with an Ag/AgCl in a saturated KCl solution reference electrode. The electrolyte was 1 M sodium hydroxide (NaOH) in DI water (pH close to 14). Figure 3(B) shows typical voltammograms measured under chopped illumination. Blue and green lines correspond to measurements recorded with specular and Lambertian back reflectors, respectively. One can see that the Lambertian back reflector gave rise to larger photocurrents than the specular one.

The photocurrent showed positive (anodic) transient peaks upon turning the light on, indicating the accumulation of holes at the photoanode/electrolyte interface. Likewise, the negative transient peaks upon light turn-off were caused by the backward recombination of electrons and holes.[26] At potentials above 1.6 V_{RHE} (V vs. the reversible hydrogen electrode), these transient peaks became small, indicating that the barrier for charge transfer from the electrode to the electrolyte was diminished by the applied potential. In the high potential regime, surface recombination was suppressed, and the current was limited by hole transfer from the hematite film to the surface. The potential range where this condition prevailed is referred to as the high-injection regime, and the corresponding net-photocurrent, which is the difference between the light (under illumination) and dark currents, is the plateau photocurrent. The plateau photocurrent is proportional to the electron-hole generation rate, that is, to the absorbed photon flux, multiplied by the internal quantum efficiency of the photoanode.[26] In this regime, the water oxidation reaction at the hematite/electrolyte interface is $4OH^- + 4h^+ \rightarrow O2 + 2H_2O$, and the complementary water reduction reaction at the counter electrode (that is, the cathode) is $4H_2O + 4e^- \rightarrow 2H_2 + 4OH^-$. The overall water splitting reaction is therefore $2H_2O +$

$4e^- + 4h^+ \rightarrow 2H_2 + O_2$, where electrons and holes are supplied by the photo-induced excitation from the valance band into the conduction band of the hematite film. In the following, we evaluate the photocurrent enhancement at an electrode potential of 1.6 V_{RHE}, well within the high-injection regime of our photoanodes as can be seen in Fig 3(B). In this case, and with the Lambertian back reflector deployed, plateau photocurrents of 0.6, 0.75, 0.86, and 0.74 mA/cm^2 were obtained for the 15, 19, 23, and 30 nm thick hematite films, respectively. These photocurrents are moderate compared to the champion hematite photoanodes reported to date that achieved more than 4 mA/cm^2.[27,28] This is because the photoanode was not optimized for high performance. Nevertheless, we can still analyze the relative enhancement in photocurrent and light harvesting (absorption) and compare the different scenarios with Lambertian vs. specular back reflectors. By relative enhancement, we mean the ratio of some measured property obtained with a Lambertian reflector attached to the backside of the cell divided by the same property measured with the specular mirror attached to it instead of the Lambertian reflector. The analyzed properties were the light absorption and photocurrent. Besides light absorption, all the other processes that influence the photocurrent, such as charge separation, transport and injection, remained unaffected by the type of the reflector attached to the backside of the cell, and therefore they did not affect the relative enhancement. This way, we can analyze the optical enhancement induced by the Lambertian light trapping with respect to the trivial enhancement induced by a specular back reflector, with no spurious effects that were not related to the light management scheme. The effect of different light management schemes, that is Lambertian vs. specular back

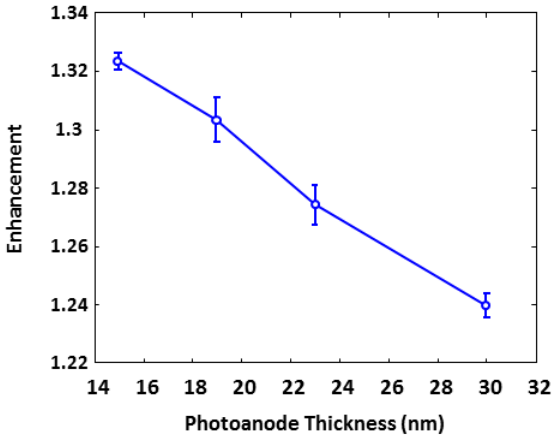

Fig. 4. Photocurrent enhancement obtained for a Lambertian back reflector relative to a specular one.

reflectors, is expected to prevail for high performance photoanodes, as well as for ones with moderate performance, as long as the structure of the cell (and the hematite film thickness) remains the same. Figure 4 shows the relative enhancement in photocurrent vs. hematite film thickness for the entire collection of photoanodes. The errors arose from the repeated installation of the same photoanode into the test cell and the refreshment of the electrolyte. The relative enhancement increased with decreasing film thickness, from 24% for the 30 nm thick film and up to 32% for the 15 nm thick film. This trend resulted from the larger absorption of the thicker films that left less light to be scattered, then to be trapped by TIR (total internal reflection), and eventually to be absorbed by the hematite film. Figure 4 clearly demonstrates the advantage of our light trapping scheme that led to significant enhancement in the photocurrent, well above the trivial employment of specular back reflectors.

Discussion

As mentioned earlier, the reason for considering the relative enhancement rather than the absorptance or photocurrent values is because the relative enhancement depends only on the light management and not on the photoelectrochemical properties of the photoanode. This is because the charge transport, separation and injection yields are insensitive to the type of reflector attached to the backside of the cell, and therefore, these effects are normalized out when considering the relative enhancement. Nevertheless, rigorous quantitative analysis of the optical effects that take place in our device is still challenging. First, the cell comprises a multilayer optical stack with individual layer thicknesses spanning a range of values that are orders of magnitude apart. For example, the thickness of the glass substrates is about a millimeter, whereas the hematite films are only 15 to 30 nm thick. This mismatch disables the direct numerical integration of Maxwell's equations by the finite element[30] or finite-difference[31,32] methods that are commonly employed for the analysis of Lambertian reflectors. We also found that ray-optics modules do not account faithfully for the absorption of ultrathin layers such as the hematite films considered here. Second, Lambertian reflections are stochastic in nature. This prohibits the use of the optical transfer matrix formalism (or the equivalent scattering matrix) that represents the exact solution of Maxwell's equations for structures with an infinite lateral extent and for coherent light propagation.[32] This challenge could partially be resolved by employing rigorous coupled wave analysis methods,[33] scattering models of various typs,[34,35] or radiative transfer formalisms,[36] all of which can handle the stochastic nature of Lambertian scattering. However, these methods cannot cope with the finite extent of the optical stack considered here. Therefore, we are left with the generic expression relating the absorptance of the cell (A) to the single pass absorptance (a) and the confinement factor (f):[11]

$$A = \frac{a}{a + 1/f} \quad . \qquad (1)$$

The above relation results from balancing the internal and external photon fluxes. As such, it can cope with irregular shapes, material compositions and reflector arrangements, as long as the confinement factor f can be properly identified. Indeed, the origin of this formalism lies with the analysis of low absorptivity PV cells,[10] and it was later extended to account for parasitic absorption[37] and high absorptive media,[11] and was even recently applied to PV modules placed in an external cavity.[38] In the following, we develop a quantitative model based on this formalism. It is noteworthy that the single path absorption, a, includes both work-producing and parasitic optical losses. The Lambertian light trapping enhances both of these losses, as becomes evident from Eq. (1).

Let us consider, for example, a simple slab with absorptivity α, refractive index n, and thickness L, illuminated with collimated light and having a Lambertian back reflector. The single pass absorptance in this case is $a = 1 - \exp(-\alpha L) \approx \alpha L$ where the last equality holds for ultrathin slabs with low absorptivity ($\alpha L < 1$). The confinement factor in this case was extensively studied,[10,11] so it suffices to mention that bi-directional propagation yields a factor of two, longer ray paths due to angular propagation yield another factor of two, and TIR yields another factor of n^2; thus, in the end, the overall enhancement factor is $4n^2$. From Eq. (1), the low absorptivity limit yields an effective absorptance that approaches $A = 4n^2\alpha L$.[10] In our case, however, $2n^2$ is a more appropriate limit since we consider the relative enhancement due to Lambertian scattering with respect to bi-directional propagation induced by a specular back reflector. An obvious drawback of having a bi-directional propagation is that, unlike in the resonant trapping method,[8] not all charge carriers are photogenerated close to the desired hematite/electrolyte interface. This bi-directionality is a fundamental outcome of the Lambertian light trapping; thus, it can be considered as the price paid for moving the back reflector away from the corrosive proximity of the electrolyte.

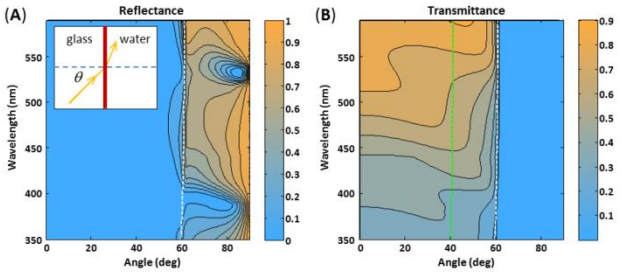

Fig. 5: Calculated reflectance (A) and transmittance (B) for a glass/FTO/SnO_2/hematite/water stack illuminated from the glass side. The calculation domain is shown in the inset: The light ray, marked in orange, propagates at an angle θ from the glass to the water via the FTO/SnO_2/hematite stack that is shown in red.

An analysis according to Eq. (1) requires a clear distinction between the thick and thin compartments of the cell. The thick parts are the glass substrate, front window, and electrolyte layer; all of them are about 1 mm thick, and they are optically lossless. The electrolyte is assigned the refractive index of water (n = 1.33). The thin regions include the FTO layer (~350 nm thick), SnO_2 layer (~40 nm thick), and the hematite film whose thickness ranges from 15 to 30 nm. These thin regions are also the lossy parts of the cell, and because they are so thin with respect to the lossless thick parts, they are considered as surface losses within the ray-optics analysis. Surface absorption, in this case, is proportional to the layer thickness through the single pass absorptance (a).

TIR, an essential key for Lambertian light trapping, occurs when rays from a high index medium impinge on an interface with a low index medium. In our case, light enters the PEC cell as a collimated beam, traverses the cell, and then scatters hemispherically by the Lambertian back reflector. The scattered light then encounters two TIR events as it propagates backwards through the cell. The first TIR is at the photoanode/electrolyte interface, and the second one takes place at the interface between the front window and the air outside the cell. Let us analyze the properties of the first interface, where TIR is less obvious due to optical losses from absorption in the hematite film. Toward this end, we calculated the angle- and wavelength-dependent normalized power reflection from a glass/FTO/SnO_2/hematite/water optical stack. The calculations were made with the transfer matrix formalism[32] using an exact model of the TEC substrate[39] coated with a 19 nm hematite film under the assumption of an infinite lateral extent of the layers. In this case, the light traversed the FTO/SnO_2/hematite layer at an angle θ from the glass side into the water, as shown in the inset of Fig. 5(A) (no back reflector is present). The reflection of unpolarized light was obtained by averaging the reflections of the TE and TM polarizations. The results are shown in Fig. 5(A) wherein the wavelength dependence of the critical angle at the glass/water interface is also shown, for comparison, by the dashed white line. The region to the right of this line is where TIR at the glass/water interface occurs with no intermediate lossy layers. The reflectance map in Fig. 5(A) shows the effect of losses; at longer wavelengths, where losses are low, TIR provides a good approximation of the actual conditions, with the exception of the low reflectance spot centered at 85° and 533 nm that results from interference in the FTO layer. This confinement by TIR forms the first trapping mechanism in our device.

Fig 5(B) complements Fig 5(A) in that it shows the normalized transmittance to the electrolyte (water) from the glass and through the FTO and hematite layers. As before, TIR at the glass/water interface is shown with a dashed white line. The fact that there is hardly any transmittance above the critical angle for TIR (at about 60°) indicates that unreflected light was absorbed in the lossy components of the cell (that is, the FTO,

SnO_2, and hematite layers). As expected, below the critical angle for TIR, there is finite transmittance that rises at longer wavelengths where the optical losses due to absorption are small. This transmitted light propagates in the electrolyte toward the glass window occupying a full hemispherical range of angles. Upon transmission to the glass window, some reflection occurs, but it is relatively small due to the low refractive index of water (n = 1.33) and glass (n = 1.48). For example, reflectance values close to 10% for the TE polarization and close to 5% for the TM polarization are expected at an angle of 70°. Thus, the reflectance at this interface is small, for the most part, and therefore, it makes only a small contribution to the light trapping effect. The front window and the substrate are both made of glass. This means that the light there propagates at angles no larger than that defined by the first TIR event, which is about 60°. The TIR from the glass and into the air, however, occurs at about 40°, as shown by the dashed green line in Fig. 5(B). This shows that a significant amount of light from the Lambertian reflection that reaches the front widow cannot escape the cell, and it is directed backwards into the cell by the second TIR event. This is the second trapping mechanism of our device. Since the glass/air interface has a higher refractive index contrast than the glass/water interface with a critical angle of 40° relative to 60°, respectively, this event determines the ultimate level of light trapping in our device. These two mechanisms trap light in the interior of the cell for repeated interaction with the hematite, but also for parasitical loss mechanisms (mainly at the FTO electrode, back reflector, and wasted absorption in the hematite film due to charge recombination).

Thus, as far as light trapping is concerned, an enhancement of up to $2n_{glass}^2 \approx 4.5$ is expected for ultrathin films with $\alpha L < 1$.

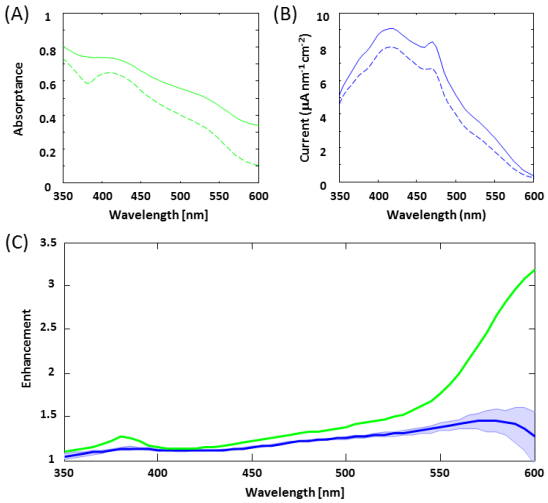

Fig. 6: Absorptance (A), plateau photocurrent (B) and relative enhancement spectra (C) obtained for the 19 nm thick hematite photoanode. Green and blue curves indicate absorptance and plateau photocurrent spectra, respectively, whereas solid and dashed lines correspond to results obtained with the Lambertian and specular back reflectors, respectively. The shaded region in panel C corresponds to the measurement errors.

However, the photocurrent enhancement values in Fig. 5 are much smaller than that, suggesting that another loss mechanism is at play. This loss comes from light escape through the cell edges. Since the thickness of our cell is not negligible with respect to its diameter (3 vs. 40 mm, respectively), the side area is quite significant with respect to the surface area. This means that light that is scattered or undergoes one of the TIR events close to the cell edges is likely to escape sideways rather than reaching the hematite film. This escape loss is at play for the Lambertian back reflector but not for the specular one. Indeed, noticeable light escape from the side facets was observed from the illuminated cell when it was fitted with a Lambertian back reflector. Putting all these mechanisms together, along with their mutual interactions, makes optical analysis of our device challenging.

Let us examine how these optical confinement and loss mechanisms play a role in the light harvesting and photocurrent generation that give rise to the respective relative enhancements in the 19 nm thick hematite photoanode. The empirical results, that is the absorptance, plateau photocurrent (measured at 1.6 V_{RHE}), and relative enhancements obtained for this photoanode, are shown in Fig. 6. Panel (A) shows the absorptance spectra obtained with Lambertian and specular back reflectors, presented by solid and dashed line curves, respectively. In both cases, the absorptance increased with decreasing wavelengths, in agreement with the hematite absorption coefficient from Fig. 3(A). More importantly, however, is the fact that the absorptance with the Lambertian back reflector was consistently larger than that obtained with the specular one, at nearly all wavelengths from 350 to 600 nm (see Fig. 6A). The difference in the reflectance of the respective back reflectors cannot account for the enhancement in absorptance at wavelengths above ~420 nm because their absorptance was nearly the same in this range (see Fig. 3A). Thus, it must be due to the Lambertian scattering effect. Similarly, the photocurrent obtained with the Lambertian back reflector was consistently higher than that obtained with the specular one (see Fig. 6B). Fig. 6(C) shows the relative enhancement in the absorptance (green curve) and photocurrent (blue curve). The shaded zone indicates measurement errors caused by repeated installation of the photoanode onto the cell and refreshment of the electrolyte (the errors in the absorptance were negligible). The photocurrent enhancement spectrum clearly shows characteristics that are expected for Lambertian light trapping. At short wavelengths (< 400 nm), the absorptance was already high for the first pass through the photoanode, and therefore, the enhancement was quite small. At longer wavelengths, the single pass absorptance became small, and therefore, light confinement by TIR resulted in substantial enhancement.

Beyond 580 nm, the photocurrent enhancement dropped down because the absorption edge (bandgap) of the hematite photoanode was approached. Low photocurrents led to larger experimental errors (see shaded area in Fig. 6C). Nevertheless, the absorptance enhancement continued to rise because it also included spurious optical losses in the cell. At 600 nm, the single pass absorptance was very small, and the absorptance enhancement reached a factor of ~3.25, close to the ultimate $2n^2$ limit of 4.5 for our cell.

It is noteworthy that the absorptance enhancement exceeded the photocurrent enhancement. The difference was quite small at short wavelengths, but it increased with increasing wavelengths and became quite significant above 500 nm and even more so above 550 nm (see Fig. 6C). Since we were dealing with a relative enhancement of the same cell wherein the only difference was the type of back reflector attached to the cell, this discrepancy must have been due to an optical effect. This effect can be attributed to the opposite influence of light escape through the cell edges on the absorptance and photocurrent enhancements. In case of the photocurrent enhancement, the escaped light was deprived from the hematite photoanode, and therefore, the photocurrent was reduced. Light escape with the Lambertian back reflector was more significant than with the specular one. Therefore, the full potential of the Lambertian light trapping method is underestimated in this case due to light escape through the edges. At the same time, the escaped light was not directed back into the integrating sphere, and therefore it was falsely registered as being absorbed, giving rise to a false overestimate of the enhancement in optical absorptance in our cell.

We now turn to estimate the potential photocurrent enhancement when light escape from the cell edges was prevented. The absorptance of cells fitted with either the Lambertian or specular back reflectors is accounted for by Eq. 1. Thus, the relative enhancement in absorptance is:

$$E_{Opt} = \frac{A_L}{A_S} = \frac{a + 1/2}{a + 1/f_{Opt}} \quad . \tag{2}$$

where A_L and A_S denote the absorptance with Lambertian and specular back reflectors, respectively, a is the single pass absorptance through the cell, and f_{Opt} is the confinement factor induced by the Lambertian back reflector. This factor emerges from the interplay between the two light trapping mechanisms and the edge losses. The confinement factor for the specular case is taken as 2 due to the double optical path length compared to the single path length without the back reflector. For low absorptance, Eq. (2) reduces to $E_{Opt} = f_{Opt}/2$. The importance of Eq. (2) is that it relates the effective confinement to the experimentally observed enhancement. In a similar manner, we can also write for the photocurrent enhancement:

$$E_{Curr} = \frac{I_L}{I_S} = \frac{EQE \times A_L}{EQE \times A_S} = \frac{a + 1/2}{a + 1/f_{Curr}} \quad . \tag{3}$$

The difference between Eqs. (2) and (3) is in how light escape through the cell edges influences the respective confinement factors. As explained before, mounting the cell against the integrating sphere meant that the light that escaped through the edges was registered as being absorbed. This is due to the relation $A = 1 - R$ (since no transmission existed). Therefore, the escaped light falsely increases f_{Opt}, but in reality, it decreases the amount of light absorbed in the cell and the photocurrent produced by the cell, and therefore f_{Curr} decreases. Without edge losses, $f_{Opt} = f_{Curr}$, and therefore, we write the "true" confinement factor as:

$$f = f_{Opt}/L_{Edge} = f_{Curr} \times L_{Edge} \quad , \tag{4}$$

where L_{Edge} is the loss due to light escape through the edges. From Eq. (4), we obtain the following relation between f_{Opt}, f_{Curr} and L_{Edge}:

$$L_{Edge} = \sqrt{f_{Opt}/f_{Curr}} \quad . \tag{5}$$

Using this value, the "true" confinement factor f can be calculated and inserted into Eqs. (3) and (4) in order to estimate the relative absorptance and photocurrent enhancements, respectively, had edge losses been prevented. Fig. 7 shows the corrected "true" enhancement spectrum (solid black line) that was calculated for the 19 nm thick hematite photoanode using the results from Fig. 6(C). The edge loss parameter, L_{Edge}, is shown by the dashed black line. As expected, it increased at longer wavelengths where the absorption was low. For comparison, the uncorrected relative enhancements in absorptance and photocurrent are shown by the green and blue curves, respectively. As expected, the "true" enhancement lay

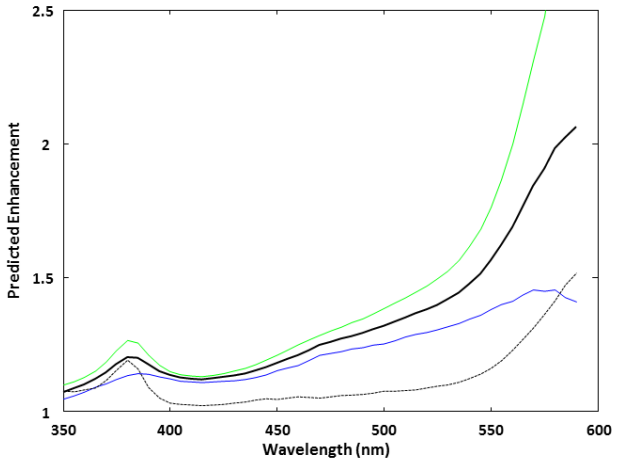

Fig. 7: The corrected enhancement spectrum (solid black line) of the 19 nm thick hematite photoanode. The uncorrected absorptance and photocurrent enhancement spectra are also shown, for comparison, by the green and blue curves. The dashed black line curve shows the edge loss factor, L_{Edge}.

somewhere between the measured (uncorrected) photocurrent and absorptance enhancements. It is noteworthy that the single path absorption, *a*, that was obtained from the experimental data included both work-producing and parasitic absorptions. The use of a specular silver mirror as a reference back reflector ensured that the amount of parasitic losses remained nearly the same upon swapping the two back reflectors. Figure 1(B) shows that indeed this was the case, for the most part, at least for wavelengths longer than 425 nm. Thus, for this range of wavelengths, the single path absorption was considered to be identical in both cases, and the only difference that arose due to swapping the back reflectors was the onset of confinement and the inevitable edge losses that followed.

Finally, we follow these calculations in order to estimate the potential photocurrent enhancement without any edge losses, $\tilde{\tilde{E}}$. This is calculated using the following formula:

$$\tilde{\tilde{E}} = \frac{\int A_{Lamb}(\lambda) S_{AM1.5}(\lambda) d\lambda}{\int A_{Spec}(\lambda) S_{AM1.5}(\lambda) d\lambda}, \quad (6)$$

where A_{Lamb} and A_{Spec} are the measured absorptance spectra obtained with Lambertian and specular back reflectors and $S_{AM1.5}$ is the AM1.5G spectrum illumination.[40] The results are shown in Fig. 8 (black line). For comparison, we also show the photocurrent enhancement values measured for the four photoanodes (dashed blue line curve). The figure shows that the edge losses became more severe as the film thickness was reduced. This is because the single path absorptance became lower with decreasing film thicknesses. However, these losses could be effectively diminished by increasing the cell diameter.

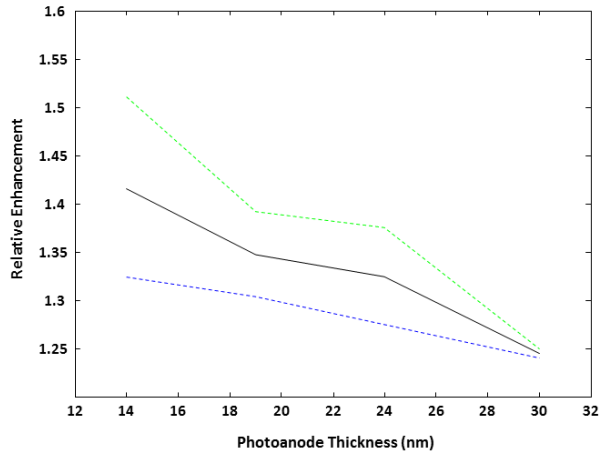

Fig. 8: Predicted photocurrent enhancement (relative to specular back reflector) without edge losses (solid black line) and measured photocurrent enhancement (dashed blue line) as a function of the hematite film thickness.

Without edge losses, relative enhancements as large as 42% are expected for a 15 nm thick hematite photoanode.

Conclusions

Photocurrent enhancements of 24% to 32% were obtained for photoanodes with hematite film thicknesses ranging from 30 to 15 nm, respectively, by using a Lambertian back reflector relative to the photocurrent obtained with a specular back reflector. These enhancements were obtained despite a slightly higher reflectance of the specular mirror (by as much as 3%) in the relevant spectral range (400-590 nm). This shows that the Lambertian light trapping method can be applied to enhance the performance of ultrathin deep-subwavelength films. The apparent contradiction between the ray-optics nature of the Lambertian light trapping mechanism and the subwavelength thickness of the photoactive material is resolved by separating the confinement and absorption sites within the macroscopic cell. This separation results in a simple and cost-effective method that is additive to other techniques for improving the optics of solar cells, be it at the photoanode itself[8,41] or at the periphery of the cell.[42]

By comparing the absorptance and photocurrent enhancements, we have identified and quantified the deleterious effect of light escape through the cell edges. The analysis shows that photocurrent enhancement as high as 42% is expected for a 15 nm thick hematite film, relative to the photocurrent obtained with a specular back reflector. However, in practice, the enhancement was significantly smaller, 32%, due to edge losses. The edge losses increased with decreasing hematite film thickness, but they are expected to decrease with increasing photoanode diameter.

Ultimately, the enhancement induced by the Lambertian light trapping is determined by the refractive index contrast of the material where ray randomization initially takes place, the glass substrate in our case, and the ambient air. Using high-index transparent substrates could, therefore, produce stronger light trapping and higher photocurrent enhancements, beyond the prevention of edge losses.

The spatial separation of absorption and confinement sites may also benefit other devices in which absorption of a subwavelength photoactive layer needs a boost, such as organic solar cells. Another useful merit of this light management method is that it works with simple, durable commercial components (white diffuser sheets), thereby enabling the competitive and simple application of this approach to other types of thin film solar cells and photodetectors.

Acknowledgements

The research leading to these results has received funding from the European Research Council under the European Union's

Seventh Framework Programme (FP/2007-2013) / ERC Grant Agreement n. [617516] and from the Israeli Nanotechnology Focal Technology Area on Nanophotonics for Detection. Measurements were conducted at the Technion's Photovoltaic Laboratory, supported by the Nancy & Stephen Grand Technion Energy Program (GTEP) and by the Russell Berrie Nanotechnology Institute (RBNI), and at the Technion's Hydrogen Technologies Research Laboratory (HTRL), supported by the Adelis Foundation and by the Solar Fuels I-CORE program of the Planning and Budgeting Committee and the Israel Science Foundation (Grant n. 152/11). This work was also supported by the Grand Technion Energy Program (GTEP), and constitutes part of The Leona M. and Harry B. Helmsley Charitable Trust reports on Alternative Energy series of the Technion, Israel Institute of Technology, and the Weizmann Institute of Science.

The authors would like to thank Dr. Guy Ankonina for helping with the optical measurements and Yosef Mahfuda for the construction of the modular PEC cell.

References

1 J. A. Bard, M. A. Fox, *Acc. Chem. Res.* 1995, **28**, 141-145.
2 N. S. Lewis, D. G. Nocera, *Proc. Natl. Acad. Sci. USA* 2006, **103**, 15729-15735.
3 M. J. Katz, S. C. Riha, N. C. Jeong, A. B. Martinson, O. K. Farha, J. T. Hupp, *Coord. Chem. Rev.* 2012, **256**, 2521-2529.
4 B. Gilbert, C. Frandsen, E. R. Maxey, D. M. Sherman, *Phys. Rev. B* 2009, **79**, 035108.
5 D. K. Bora, K. Debajeet, A. Braun, E. C. Constable, *Energy Environ. Sci.* 2013, **6**, 407-425.
6 N. J. Cherepy, D. B. Liston, J. A. Lovejoy, H. Deng, J. Z. Zhang, *J Phys. Chem. B* 1998, **102**, 770-776.
7 I. Cesar, K. Sivula, A. Kay, R. Zboril, M. Grätzel, *J. Phys. Chem. C* 2008, **113**, 772-782.
8 H. Dotan, O. Kfir, E. Sharlin, O. Blank, M. Gross, I. Dumchin, G. Ankonina, A. Rothschild, *Nat. Mat.* 2013, **12**, 158-164.
9 B. Chalmers, R. King, R. Shuttleworth, *Proc. R. Soc. Lond. Ser. A* 1948, **193**, 465-483.
10 E. Yablonovitch, *JOSA* 1982, **72**, 899-907.
11 M. A. Green, *Prog. Photov.* 2002, **10**, 235-241.
12 K. R. Catchpole, A. Polman, *Opt. Exp.* 2008, **16**, 21793-21800.
13 I. Thomann, B. A. Pinaud, Z. Chen, B. M. Clemens, T. F. Jaramillo, M. L. Brongersma, *Nano Lett.* 2011, **11**, 3440−3446.
14 J. Li, S. K. Cushing, P. Zheng, F. Meng, D. Chu, N. Wu, *Nat. Commun.* 2013, **4**, 2651.
15 E. Thimsen, F. Le Formal, M. Grätzel, S. C. Warren, *Nano lett.* 2010, **11**, 35-43.
16 A. Polman, H. A. Atwater, Nat. Mat. 2012, **11**, 174-177.
17 S. Mokkapati, K. R. Catchpole J. App. Phys. 2012, **112**, 101101.
18 J. Zhu, C. Hsu, Z. Yu, S. Fan, Y. Cui, *Nano Lett.* 2009, **10**, 1979-1984.
19 J. Grandidier, D. M. Callahan, J. N. Munday, H. A. Atwater, *Adv. Mater.* 2011, **23**, 1272-1276.
20 K. X. Wang, Z. Yu, V. Liu, M. L. Brongersma, T. F. Jaramillo, S. Fan, ACS Photonics 2014, **1**, 235-240.
21 V. Ganapati, O. D. Miller, E. Yablonovitch *IEEE J PHOTOVOLT* 2014, **4**, 175-182.
22 J. N. Munday, D. M. Callahan, H. A. Atwater, *Appl. Phys. Lett.* 2012, **100**, 121121.
23 Z. Yu, A. Raman, S. Fan, *PNAS* 2010, **107**, 17491-17496.
24 C. Battaglia, C. Hsu, K. Söderström, J. Escarré, F. Haung, M. Charriére, M. Boccard, M. Dspeisse, D. T. L. Alexander, M. Cantoni, Y. Cui, C. Ballif, *ACS nano* 2012, **6**, 2790-2797.
25 Kirtiman Deo Malviya, Hen Dotan, Ki Ro Yoon and Il-Doo Kim, and Avner Rothschild, *J. Mater. Res.* 2015, DOI: 10.1557/jmr.2015.300.
26 H. Dotan, K. Sivula, M. Grätzel, A. Rothschild, S. C. Warren, *Energ. Environ. Sci.* 2014, **4**, 958-964.
27 S. C. Warren, K. Voïtchovsky, H. Dotan, C. M. Leroy, M. Cornuzl, F. Stellacci, C. Hébert, A. Rothschild, M. Grätzel, *Nat. Mater.* 2013, **12**, 842–849.
28 J. Y. Kim, G. Magesh, D. H. Youn, J. Jang, J. Kubota, J. S. Lee *Sci. Rep.* 2013, **3**, 2618 1-8.
29 P. Kowalczewski, M. Liscidini, L. C. Andreani, *Opt. lett.* 2012, **37**, 4868-4870.
30 J. Lacombe, O. Sergeev, K. Chakanga, K. von Maydell, C. Agert, *J. Appl. Phys.* 2011, **110**, 023102.
31 B. C. P. Sturmberg, K. B. Dossou, L. C. Botten, A. A. Asatryan, C. G. Poulton, R. C. McPhedran, C. Martijn de Sterke, *Opt. Exp.* 2013, **21**, A964-A969.
32 M. Born, E. Wolf, *Principles of Optics,* Cambridge University Press 1999, 54-64.
33 S. Schröder, A. Duparré, L. Coriand, A. Tünnermann, D. H. Penalver, J. E. Harvey, *Opt. Exp.* 2011, **19**, 9820-9835.
34 C. Battaglia, C. Hsu, K. Söderström, M. Charrière, M. Boccard, M. Despeisse, D. T. L. Alexander, M. Cantoni, Y. Cui, C. Ballif, F. Haug, *J. Appl. Phys.* 2012, **112**, 094504.
35 K. Jäger, M. Fischer, R. Van Swaaij, M. A. Zeman, *J. Appl. Phys.* 2012, **111**, 083108.
36 N. Dahan, Z. Jehl, J. F. Guillemoles, D. Lincot, N. Naghavi, J. J. Greffet, *Opt. Exp.* 2013, 21, 2563.
37 J. Gee, *Proceedings of the 20th IEEE Photovoltaic Specialists Conference* 1988, 549–554.
38 L. A. Weinstein, W. Hsu, S. Yerci, S. V. Boriskina, G. Chen, *J. Opt.* 2015, **17**, 055901.
39 S. Kohli, M. Mankatesan, J. N. Hilfiker, P. R. McCurdy, R. A. Enzenroth, K. L. Barth, W. P. Smith, R. Luebs, W. S. Sampath, *J. Sol. Eng.* 2009, **131**, 021009.
40 ASTM G173 – 03 (2012), *Standard Tables for Reference Solar Spectral Irradiances: Direct Normal and Hemispherical on 37° Tilted Surface* (DOI: 10.1520/G0173-03R12).
41 Y. Qiu, S. Leung, Q. Zhang, B. Hua, Q. Lin, Z. Wei, K. Tsui, Y. Zhang, S. Yang, and Z. Fan, *Nano Lett.* 2014, **14**, 2123−2129.
42 M. M. Tavakoli, K. Tsui, Q. Zhang, J. He, Y. Yao, D. Li, and Z. Fan, *ACS Nano* 2015, **9**, 10287-10295.